IOP PUBLISHING SEMICONDUCTOR SCIENCE AND TECHNOLOGY

Semicond. Sci. Technol. **23** (2008) 123001 (18pp) doi:10.1088/0268-1242/23/12/123001

TOPICAL REVIEW

Strong exciton–photon coupling in semiconductor quantum dot systems

Johann Peter Reithmaier

Technische Physik, Institute of Nanostructure Technologies and Analytics, University of Kassel, Heinrich-Plett-Str 40, 34132 Kassel, Germany

Received 10 April 2008, in final form 8 July 2008
Published 29 October 2008
Online at stacks.iop.org/SST/23/123001

Abstract

An overview is given on strong coupling phenomena in semiconductor quantum dot systems by utilizing cavity-enhanced light–matter interaction. The basic theory on strong coupling, the quantum dot and cavity fabrication technologies are reviewed while mainly three approaches are highlighted, i.e., micropillar, photonic crystal and microdisc cavities. The first and recent strong coupling experiments and the impact for future work are discussed.

(Some figures in this article are in colour only in the electronic version)

1. Introduction

The basis of any quantum information processing is the ability of a quantum system to couple coherently to different quantum states by suppressing any interaction with the environment. Coherent or strong coupling of quantum states means here the exchange of energy between two quantum states without loosing the phase relationship between the individual wavefunctions. The isolation of electronic quantum states of single atoms localized in magnetic traps seems a straightforward method for the preparation and control of quantum states [1]. However, the preparation and characterization of quantum states needs a controlled interaction with the environment. Optical techniques are widely used for the characterization of electronic states in ensembles of atoms or in solids, but the interaction is very weak, i.e., many interaction events have to be counted for a sufficient statistics. To enhance the light–matter interaction high-quality (Q) optical resonators were developed in different systems, which allow us to investigate the light–matter interaction down to the single particle level entering the so-called cavity quantum electrodynamics (CQED) regime [2–4].

However, it took quite some time to improve the technology to a level, which allows us to achieve the strong coupling condition at the single particle quantum limit. In 2004, three groups obtained independently the first time a coherent coupling between a single photon confined in a high-Q optical cavity and a localized electronic or excitonic quantum state, respectively, by using three different approaches, i.e., a single trapped atom in a microwave cavity, [5] a semiconductor quantum dot embedded in a micropillar cavity [6] and in a photonic crystal (PC) membrane microcavity [7]. One year later strong coupling was also achieved in microdiscs [8]. A brief summary and comparison about all four approaches are made by Khitrova *et al* [9].

This paper will give an actual review about strong coupling phenomena at the quantum limit in semiconductor quantum dots mainly based on the enhanced light–matter interaction in optical microcavities. The paper is divided into three major sections starting with an introduction to basic theory of CQED followed by an overview of different fabrication technologies and corresponding experimental findings.

2. Theoretical background

Let us consider the enhancement effect of the light–matter interaction by three-dimensionally confined photon modes in high-Q cavities. In figure 1, a simplified illustration is shown of a single emitter (blue) in an optical cavity (optical mode indicated in red). In reality the emitter could be a semiconductor quantum dot, where electron–hole recombination takes place via dipole interaction with the confined light field. The cavity, e.g., may consist of a semiconductor with a larger bandgap than the quantum dot material and the facets have to be highly reflective.

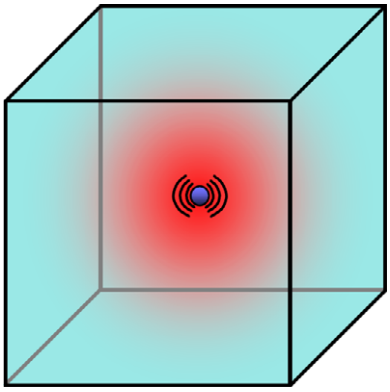

Figure 1. Illustration of a dot-like single light emitter (blue) positioned at the maximum field amplitude of the three-dimensionally confined fundamental mode (red) of a box microcavity with volume V. (Colour online only.)

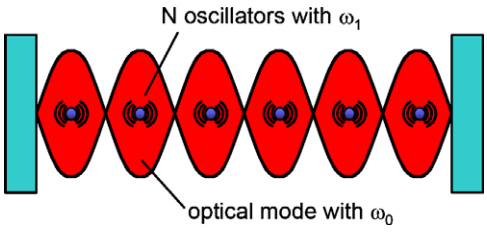

Figure 2. Illustration of N interacting oscillators with a single optical mode in a cavity.

Due to the boundary conditions, by the cavity facets and the limited structure size in the order of only a few wavelengths of the emitted light, the optical modes are fully discretized [10]. By neglecting leaky modes, a recombination process in the emitter can only occur if the transition energy fits with the energy of the optical cavity resonances. This leads to the non-classical effect that the spontaneous emission can be strongly enhanced (in-resonance) or suppressed (off-resonance) [11–13]. A theoretical review about nonlinear optics in semiconductor microcavities is given by Khitrova *et al* [14].

2.1. Simplified harmonic oscillator model

This basic interaction between single emitters, e.g., excitons as excited quantum dot states and empty cavity modes, can be modelled in a simplified way by the interaction of harmonic oscillators [15, 16]. Rudin and Reinecke calculated this problem by a classical as well as by a quantum mechanical approach, which leads to identical relationships assuming only a linear interaction [15].

Let us assume, as illustrated in figure 2, that N oscillators with identical angular frequency ω_1 interact linearly with a single optical mode represented by the angular frequency ω_0. If one neglects in a first step any dissipative phenomena, the Hamiltonian is given by [15]

$$H_{\mathrm{osc}} = \frac{p_0^2}{2} + \frac{\omega_0^2}{2}x_0^2 + \frac{1}{2}\sum_{i=1}^{N}\left(p_i^2 + \omega_1^2 x_i^2\right) - \alpha\sum_{i=1}^{N}(x_0 x_i) \qquad (1)$$

with p_0, x_0 being quantum mechanical operators for momentum and displacement, respectively, of the oscillator representing the optical mode and p_{i}, x_{i} as operators of the N oscillators with frequency ω_1. The last term describes the coupling between the optical mode and the other oscillators with the coupling constant α. The solution of equation (1) leads to $N-1$ degenerated eigenstates with frequencies $\Omega = \omega_1$ and two non-degenerated eigenstates with the frequencies

$$\Omega_{0,1} = \frac{1}{2}(\omega_0 + \omega_1) \mp \frac{1}{2}\sqrt{(\omega_0 - \omega_1)^2 + \frac{\alpha^2}{\omega_0\omega_1}N}. \qquad (2)$$

The frequency difference at resonant condition, i.e., for $\omega_0 = \omega_1$, gives the so-called 'Rabi oscillation frequency' with

$$\Delta\Omega = \frac{\alpha\sqrt{N}}{\omega_1}. \qquad (3)$$

This means that the Rabi frequency increases linearly with the coupling strength α and with the square root of the number N of interacting oscillators.

2.2. Single oscillator model interacting with cavity modes

As illustrated in figure 1, let us assume the interaction of a single oscillator, e.g., an exciton transition in a quantum dot, with the discrete optical modes of a high-Q cavity by taking into account energy dissipation. This dissipation can be caused by non-coherent coupling to other quantum states, like phonon coupling to the crystal lattice or the coupling to optical leaky modes as well as the escape of photons due to finite facet reflectivities.

According to Adreani *et al* [16], the interaction of a quantum dot state with the cavity mode can be modelled by a dipole interaction leading to the following interaction Hamiltonian,

$$H_1 = -\vec{d}\cdot\vec{E}, \qquad (4)$$

with $\vec{d}$ being the dipole operator and $\vec{E}$ the electric field. The electric field is quantized and can be expressed by the sum of the discrete optical modes

$$\vec{E}(\vec{r}) = \mathrm{i}\sum_{\mu}\sqrt{\frac{\hbar\omega_\mu}{2\varepsilon_r\varepsilon_0}}[\hat{a}_\mu\vec{\alpha}_\mu(\vec{r}) - \hat{a}_\mu^{+}\vec{\alpha}_\mu^{*}(\vec{r})] \qquad (5)$$

with $\hat{a}_\mu$, $\hat{a}_\mu^{+}$ being the creation and destruction operators for a cavity mode μ with frequency ω_μ, $\vec{\alpha}_\mu(\vec{r})$ normalized mode functions and ε_{r} and ε_0 the relative and vacuum permittivity, respectively. Each mode can be characterized by a quality factor Q_μ and a linewidth $\gamma_\mu = \omega_\mu/Q_\mu$ as full width at half maximum (FWHM). Using perturbation theory, the spontaneous emission rate of a dipole transition at position $\vec{r}_1$coupled to an individual cavity mode μ can be expressed by

$$\gamma_{\mathrm{SE}} = \frac{8\pi Q_\mu}{\hbar}\frac{|\vec{d}\cdot\vec{\alpha}_\mu(\vec{r}_1)|^2}{4\pi\varepsilon_r\varepsilon_0}\frac{(\gamma_\mu/2)^2}{(\omega_0-\omega_\mu)^2 - (\gamma_\mu/2)^2}. \qquad (6)$$

By assuming that the exciton dipole moment is aligned to the electric field, equation (6) can be simplified in resonance

condition (i.e., $\omega_0 = \omega_\mu$) to

$$\gamma_{SE} = \frac{8\pi Q_\mu}{\hbar}\frac{d^2}{4\pi\varepsilon_r\varepsilon_0}|\vec{\alpha}_\mu(\vec{r}_1)|^2 = F_\mu\gamma_0 \tag{7}$$

with F_μ being the Purcell factor [17] for each optical mode μ and the free decay rate γ_0, which is given by

$$\gamma_0 = \frac{4}{3}\frac{\sqrt{\varepsilon_r}}{4\pi\varepsilon_r\varepsilon_0}\frac{d^2\omega_0^3}{\hbar c^3}. \tag{8}$$

In direct relationship to the Purcell factor is the so-called spontaneous emission coupling factor β, which describes the portion of the spontaneous emission coupled into a single cavity mode:

$$\beta = \frac{F}{1+F}. \tag{9}$$

For high Purcell factors, β goes to unity, which would be identical to a threshold-less microcavity laser where each emitted photon contributes to the lasing process.

By defining a coupling constant for the exciton–photon interaction according to

$$g \equiv \frac{1}{\hbar}|\langle\vec{d}\cdot\vec{E}\rangle| \tag{10}$$

and using the oscillator strength expression

$$f = \frac{2m\omega_2 d^2}{e^2\hbar} \tag{11}$$

one can express the coupling constant g as

$$g = \sqrt{\frac{1}{4\pi\varepsilon_r\varepsilon_0}\frac{\pi e^2 f}{m_0\bar{V}}} \tag{12}$$

with m_0 being the free electron mass, e the electron charge and $\bar{V}$ the effective optical mode volume. Here it is assumed that the quantum dot is located at the field maximum.

The non-perturbative dynamics of the QD transition coupled to a cavity mode can be described by the following Hamiltonian [16]

$$H = \hbar\omega_0\hat{\sigma}_3 + \hbar\omega_\mu\left(\hat{a}_\mu^+\hat{a}_\mu + \tfrac{1}{2}\right) + \mathrm{i}\hbar(\hat{\sigma}_-\hat{a}_\mu^+ - \hat{\sigma}_+\hat{a}_\mu) \tag{13}$$

with $\hat{\sigma}_+$, $\hat{\sigma}_-$, $\hat{\sigma}_3$ being pseudospin operators for the two-level quantum dot system with ground $|g\rangle$ and $|e\rangle$ excited states, respectively. The Hamiltonian generates a ground state $|g, 0\rangle$ and a ladder of doublets with the states $|e, n\rangle$, $|g, n+1\rangle$ and $n = 0, 1, 2, \ldots$.

By simplifying the problem to the interaction of one exciton state with a single cavity mode and taking into account the finite linewidths of the exciton γ_X and cavity mode γ_C, one can derive the following two energy eigenvalues:

$$E_{1,2} = \frac{E_C + E_X}{2} - \mathrm{i}\frac{\gamma_C + \gamma_X}{4} \pm \sqrt{g^2 - \frac{(\gamma_C - \gamma_X - 2\mathrm{i}\Delta)^2}{16}} \tag{14}$$

with E_C, E_X as cavity mode energy and exciton transition energy, respectively, and $\Delta = E_X - E_C$ as a detuning factor. In resonance condition ($E_C = E_X = E_0$), the equation can be simplified to

$$E_{1,2} = E_0 - \mathrm{i}\frac{\gamma_C + \gamma_X}{4} \pm \sqrt{g^2 - \frac{(\gamma_C - \gamma_X)^2}{16}}. \tag{15}$$

Directly from equation (14) the Rabi splitting energy can be determined to be

$$\Delta E = 2\sqrt{g^2 - \frac{(\gamma_C - \gamma_X)^2}{16}}. \tag{16}$$

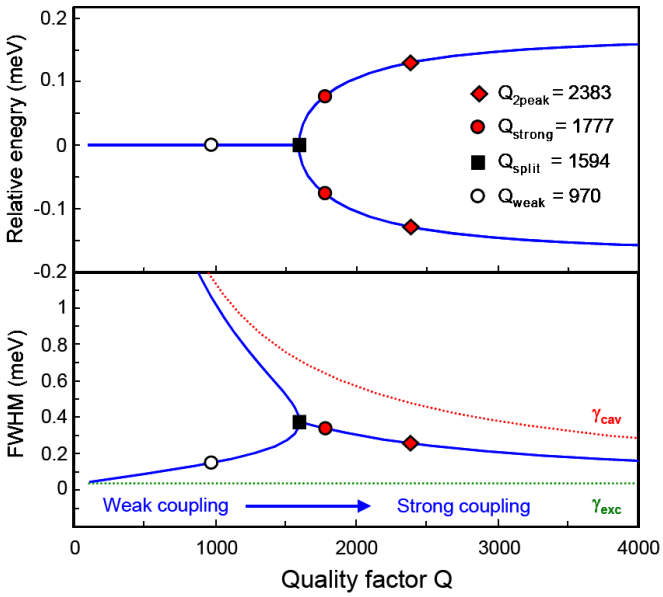

Figure 3. Calculated eigenenergies (top) and linewidths (bottom) for a two-level quantum system coupled to a single cavity. Values for specific Q-factors are indicated. Next to the linewidth of the coupled system (blue) the individual linewidths of the cavity mode (red) and of the exciton (green) are also plotted. (Reprinted with permission from [9] copyright 2006 Macmillan Publishers Ltd.) (Colour online only.)

2.3. *Transition from weak to strong coupling*

Depending on the ratio between the coupling factor g and the decay rates γ_X, γ_C of the individual oscillators, one can distinguish between the weak and strong coupling regime.

In the weak-coupling limit, i.e., for $g \ll \gamma_X + \gamma_C$, equation (15) degenerate to a single solution and the peak splitting tends to disappear. In the strong coupling limit, i.e., for $g \gg \gamma_X + \gamma_C$, two energy eigenvalues exist with a splitting energy identical to 2 g.

The transition between a weak and strong coupling can be controlled by different parameters, such as the cavity Q and the oscillator density f/V. Through equation (10) the coupling factor g can be increased by an increase of the oscillator strength f or by a decrease of the mode volume. This relationship is discussed in more detail by Adreani *et al* [16]. The cavity linewidth is inversely proportional to the Q-factor ($\gamma_C \sim 1/Q$). Therefore, by increasing the Q-factor, the cavity linewidth γ_C can be reduced, but through equation (7) the exciton linewidth γ_X will increase. However, in reality, the exciton linewidth is much smaller than the cavity linewidth, which reduces the influence of this effect.

In figure 3, the evolution of the energy eigenvalues and the linewidths of the spontaneous emission peaks are shown as a

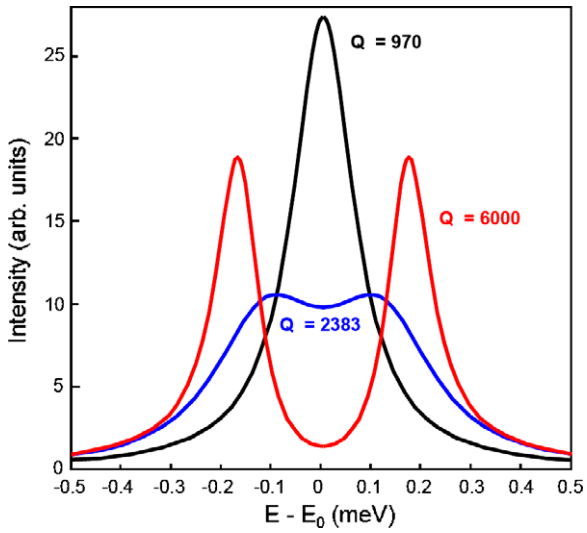

Figure 4. Calculated emission spectra for a two-level quantum system coupled to a single cavity. The black curve relates to the weak-coupling regime, while the blue and red curves relate to the strong coupling regime of figure 3. (Reprinted with permission from [9] copyright 2006 Macmillan Publishers Ltd.) (Colour online only.)

function of the cavity Q-factor according to Khitrova *et al* [9]. At low Q-values no energy splitting occurs and the exciton linewidth significantly increases while the cavity linewidth decreases below the uncoupled value of the cavity mode (cf red dotted line in figure 3). At a critical Q-value g will be larger than $|\gamma_X - \gamma_C|/4$ and the square root term in equation (15) becomes real. As a consequence, two solutions exist and the peak linewidth collapses to the same value for both peaks, which is about $(\gamma_X + \gamma_C)/2$.

In figure 4, the corresponding emission spectra are shown in the case of weak coupling (black line). Here the resonance enhancement effect is visualized. The blue curve shows the situation of strong coupling. However, the peaks are still not fully separated. Only at much higher Q-values, five times larger than the critical Q-value (red curve), the peaks are well separated due to the much narrower linewidths and larger Rabi splitting.

3. Fabrication of semiconductor quantum dots and microcavities

To reach experimentally the strong coupling regime by using semiconductor material one has to look for an adequate figure of merit, which consists of technology controllable parameters and allow us to optimize the structure in a systematic way.

According to equation (16), a Rabi splitting energy exists if the square root gets real, which leads to the following condition for strong coupling:

$$g^2 > \frac{(\gamma_C - \gamma_X)^2}{16}. \tag{17}$$

Since in most of the cases of high-Q cavity experiments, the exciton linewidth is at least one order of magnitude smaller, one can approximate equation (17) to [6]

$$g > \frac{\gamma_C}{4}. \tag{18}$$

According to equation (12) the coupling factor g is proportional to $\sqrt{\frac{f}{\bar{V}}}$. Taking into account Q-factor definition by $Q = E_C/\gamma_C$, one obtains as figure of merit for a quantum dot containing a microcavity structure

$$Q \cdot \sqrt{\frac{f}{\bar{V}}} \tag{19}$$

which has to be maximized. The Q-factor can be increased by higher mirror reflectivities and by minimizing the optical losses, e.g., caused by optical scattering or material absorption. The oscillator strength f can be increased by enlarging the number of contributing atoms, which is equivalent to the size of a quantum dot. The effective mode volume $\bar{V}$ can be decreased by reducing the microcavity size.

In the following, an overview will be given about the fabrication technologies developed to realize semiconductor microcavity structures for strong coupling experiments.

3.1. Growth of quantum dots

As emitter structures, self-assembled quantum dots or quantum dots built by quantum well interfacial fluctuations are favourized due to their defect-free crystal quality and the compatibility to embed them into semiconductor heterostructures necessary to built high-Q microcavities. Quantum dots based on interfacial fluctuations are mainly fabricated by GaAs/(Al,Ga)As quantum wells with 3–6 nm well width [18, 19]. The lateral island size is of the order of 40–50 nm [20, 21] and is therefore larger than the exciton diameter of about 30 nm in GaAs material. By depositing (In,Ga)As on GaAs self-assembled islands are formed driven by the lattice mismatch between In and non-In containing material [22–26]. The typical dimensions are in the range of 3–5 nm in height and 10–20 nm in lateral direction. The shape varies between pyramidal to half-lens shape cross sections depending on the growth conditions. In contrast to the weak electronic confinement of interfacial quantum dots, self-assembled quantum dots have a much higher potential barrier to preserve the quantization effect well above room temperature and allow the application in optoelectronics devices [27–29].

For strong coupling experiments quantum dot structures with large dipole moments are needed, which can be achieved by the fabrication of enlarged dots using special growth conditions. There are a couple of growth parameters, which influences the morphology of quantum dot structures, e.g., the amount of strained material, the growth temperature, the group V to group III ratio and the lattice mismatch, which is controlled by the In concentration [30–32]. In figure 5, secondary electron microscopy (SEM) pictures of self-assembled GaInAs dots are shown with different In concentrations starting from 60% (*a*) to 45% (*b*) down to 30% (*c*). Due to the reduced strain at 30% In content larger islands are formed and the quantum dot formation is more influenced on the crystal orientation resulting in an elongation along the [1 −1 0] direction. However, one has to take into account that a reduction of the In concentration from 100% to 30% increases also the wetting layer thickness from 0.5 nm to 2.8 nm,

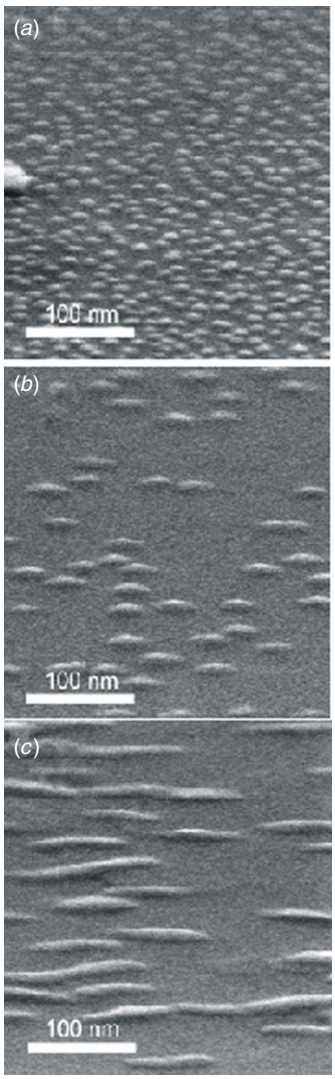

Figure 5. SEM images of self-assembled GaInAs quantum dots grown on GaAs surfaces with an In content of 60% (*a*), 45% (*b*) and 30% (*c*), respectively. From [31].

as shown in figure 6 [33]. For most of the experiments at low temperature this should not have a major impact, but the wetting layer is a possible source for decoherence at elevated temperatures by coupling to continuum states and at larger wetting layer thicknesses the effective barrier height decreases significantly.

In figure 7, a low-temperature photoluminescence spectrum ($T < 10$ K) of a quantum dot structure is shown with a 30% In concentration, where the excitation is focused to a beam diameter of about 3 μm [30]. Due to the high spatial resolution single dot lines are visible (spikes in the spectrum). Comparable dot structures were used for strong coupling experiments where the cavity mode was adjusted to the low-energy side of the spectrum to have only a spectral overlap with a few or single dots.

3.2. Realization of high-Q microcavities

The largest progress in semiconductor cavity-enhanced quantum electrodynamics in the last few years was obtained by improving the quality (Q) factor of the microcavities.

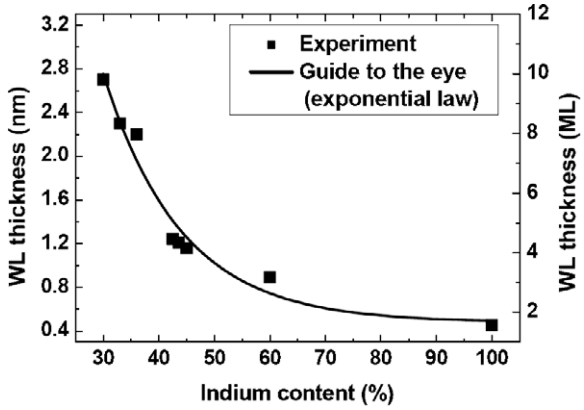

Figure 6. Wetting layer thickness as a function of the In content. From [33].

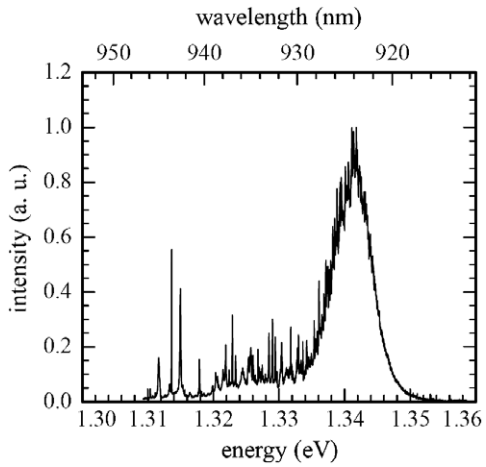

Figure 7. Low temperature photoluminescence spectra from a low In containing QD layer ($x_{In} = 30\%$) performed with high spatial resolution (excitation spot size <3 μm). From [30].

As illustrated in figure 8, three different approaches were followed, i.e., photonic crystal (PC) membrane based microcavities (*a*) [7], micropillar cavities (*b*) [6] and microdisc cavities (*c*) [8]. With all three approaches the strong coupling regime could be reached, which allowed the coherent interaction of a single photon with a single quantum dot exciton. All three approaches have special properties, which differ from each other and will be briefly discussed in the following.

3.2.1. Photonic crystal membrane cavities. Although the concept of photonic crystals is well known for two decades, [34, 35] the realization of high-quality PCs active in the optical wavelength regime seems to be rather difficult [36]. An important progress occurred by the development of membrane structures to avoid loss coupling into radiation modes vertical to the plane [37]. But the realization of high-Q cavities by implementing point defects seems to be still very challenging and it was unclear whether the limitation of Q to several thousand is related to structure imperfections or is of basic nature [38, 39]. Only since the invention of new structure design concepts in 2003 and 2005 by the pioneering work

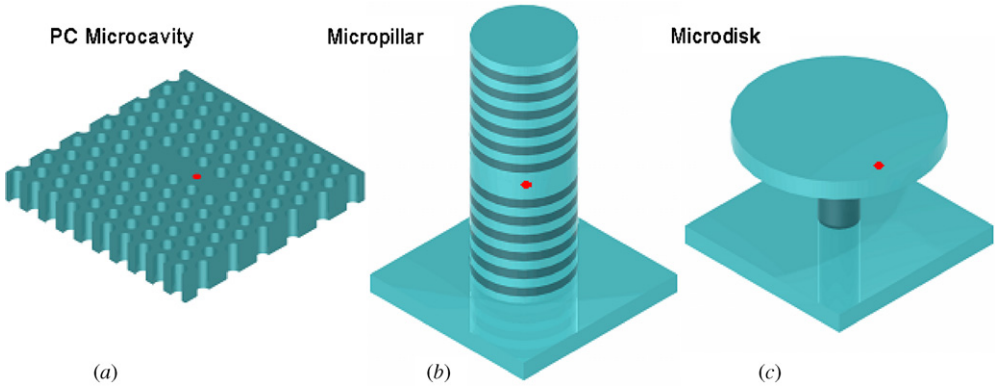

Figure 8. Illustrations of three successful microcavity designs to achieve strong coupling between a single cavity mode and an embedded quantum dot. (*a*) Photonic crystal membrane based microcavity [7], (*b*) micropillar cavity [6] and (*c*) microdisc cavity [8]. The location of the interacting quantum dot is indicated by a red dot. (Colour online only.)

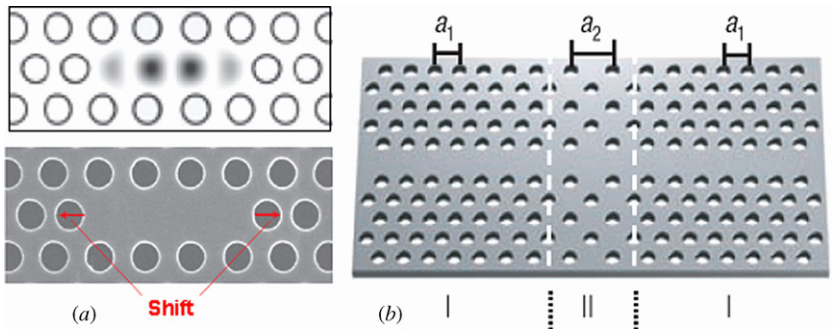

Figure 9. (*a*) Illustration of *L*3 PC cavity with shifted holes and (*b*) principle of photonic crystal heterostructure with two crystal periods (a_1, a_2). (Reprinted with permission from [44] copyright 2007 Macmillan Publishers Ltd.)

by Noda and co-workers, the Q-values could be significantly increased [40, 41]. In figure 9, the two major design concepts are illustrated. A strong improvement could be achieved by only a slight shift of the positions of the longitudinally confining two holes of an *L*3 cavity (*L*3 stands for three omitting holes) by 10% of the lattice constant. A further improvement can be achieved by following a photonic crystal heterostructure concept with a local variation of the crystal period. With this concept record values of about $Q = 2.5$ million could be demonstrated in a silicon membrane structure [42] and $Q = 300\,000$ for GaAs based membranes [43], respectively. A recent overview about spontaneous emission control by photonic crystals is given by Noda *et al* [44].

PC membrane cavities allow the realization of the smallest mode volume in the range of $V = 0.7\ (\lambda/n)^3$ and the highest Q-factors in the range $>10^7$ for passive structures. But the spatial alignment of the QDs with the mode maximum has to be in the range of <50 nm and the emission of the photon is in the PC plane, which needs more sophisticated outcoupling designs for efficient single photon collection. However, planar PC technology has the highest potential for the future realization of highly integrated quantum information processing based on single photons.

Up to now, most of the strong coupling experiments in PC microcavities are based on an arbitrary spatial overlap of a single dot with the cavity mode maximum, which needs the investigation of hundreds or more of cavities to succeed in finding a cavity shown strong coupling phenomena. To overcome this drawback, methods for pre-positioning of dots were explored. One successful approach is based on the selection of a single dot from a self-assembled dot layer with low dot densities and positioning of the PC cavity to the determined coordinates [45, 46]. To see the position of the buried dot, stacked dot structures were used, which creates a hill on the surface and which can be detected by AFM as illustrated in figure 10(*a*). The positioning accuracy in this particular case was in the range of 30 nm. Figure 10(*b*) shows the dot position relative to the cavity mode profile.

However, the spatial alignment of dots to the cavity mode is not sufficient. One needs also a spectral alignment between the cavity mode and exciton transition energy. The fine tuning over about few meV can be made by temperature tuning, as will be discussed later in section 4. To align the cavity mode over several meV, a digital etching technique was developed [45, 47] which is based on saturated oxidation of GaAs and subsequent removal. With this technique the hole diameter and the membrane thickness are modified by a few monolayers, which shifts the cavity mode digitally by 2–3 meV at each step.

An alternative tuning effect was developed by Moser *et al* who used gas condensation, like Xe or N_2 to tune the cavity mode during low-temperature investigations [48].

3.2.2. Pillar microcavities. The development of micropillar cavities results from the miniaturization of vertically surface emitting lasers (VCSELs) based on semiconductor Bragg

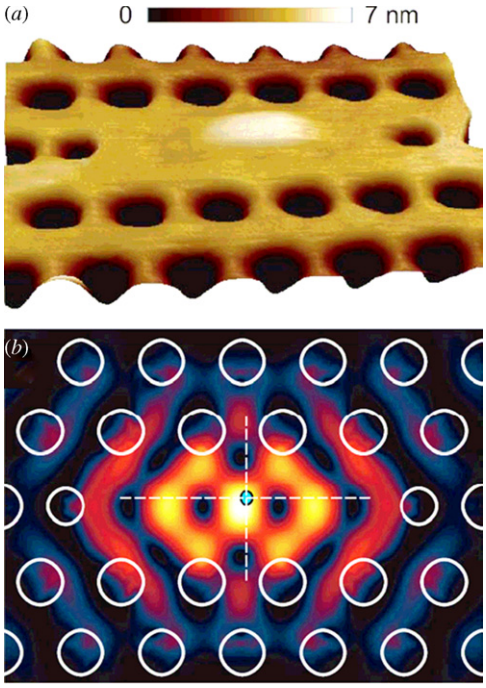

Figure 10. (*a*) AFM height plot of a PC *L*3 cavity with a hill structure, which indicates the position of the 63 nm deeply buried quantum dot and (*b*) mode simulation for the *L*3 cavity. The position of the dot is indicated by a blue dot and a dashed cross. (Reprinted with permission from [46] copyright 2007 Macmillan Publishers Ltd.) (Colour online only.)

mirrors and lateral cavity restrictions by an oxidation process of AlGaAs layers [49]. However, the lateral dimensions and the refractive index change is too low for an effective three-dimensional confinement. A full discretization of optical modes in a semiconductor microcavity in the optical domain was achieved for the first time by the fabrication of deeply etched micropillar cavities [50]. With these so-called 'photonic dots' also photonic molecules, chains, crystals and artificial defect states in photonic band gap structures could be studied by weak lateral coupling [51, 52]. Although a *Q*-factor of several thousand could be already obtained in these microcavities, which was sufficient, to observe weak and strong coupling effects with multi-electron systems like multi-quantum wells [53–56], the interaction strength was far away in achieving strong coupling effects with a single exciton state in a quantum dot.

A breakthrough could be achieved by a thorough improvement of the cavity design and micropillar etching process [6, 30, 57, 58].

In theory, the *Q*-factor of a planar cavity can be calculated according to the following formula [59],

$$Q = \frac{2L_{\mathrm{eff}}}{\lambda}\frac{\pi}{1 - r_1 r_2} \tag{20}$$

with $L_{\mathrm{eff}} \approx n_{\mathrm{cav}}\, \mathrm{d}_{\mathrm{cav}} + 2n_{\mathrm{eff}}L_{\mathrm{m}}$ being the effective cavity length, n_{cav} the refractive index of the central cavity layer, d_{cav} the cavity layer thickness, $n_{\mathrm{eff}} = 2n_{\mathrm{GaAs}}n_{\mathrm{AlAs}}/(n_{\mathrm{GaAs}} + n_{\mathrm{AlAs}})$ the effective refractive index of the DBR region, $L_{\mathrm{m}} = m_{\mathrm{eff}}(d_{\mathrm{GaAs}} + d_{\mathrm{AlAs}})$ the effective mirror length, d_{GaAs}, d_{AlAs} the layer thicknesses and $m_{\mathrm{eff}} \approx \frac{1}{2}\cdot(n_{\mathrm{GaAs}} + n_{\mathrm{AlAs}})/(n_{\mathrm{GaAs}} - n_{\mathrm{AlAs}})$ the

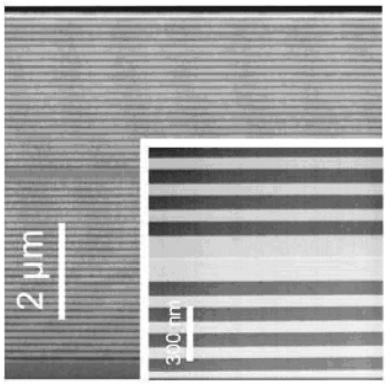

Figure 11. SEM pictures of the cross section of a vertical Bragg resonator (MC2). The inset shows a magnification of the central cavity part, where the dot layer is slightly visible as bright line. From [57].

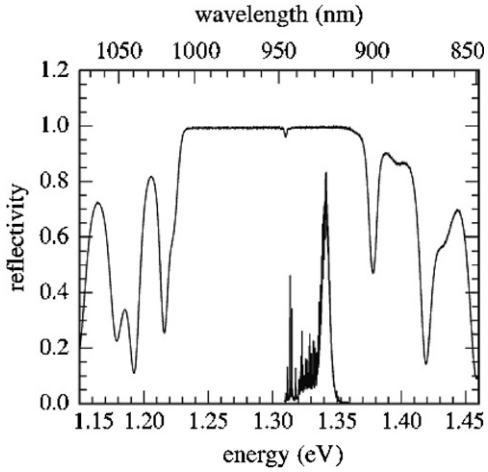

Figure 12. Reflectivity (upper line) and photoluminescence spectra of a planar cavity structure with an embedded $Ga_{0.7}In_{0.3}As$ dot layer. The dip within the stop-band of the reflectance spectrum indicates the position of the optical resonance, which coincides with single dot emissions at the low-energy side of the quantum dot spectrum. From [30].

effective number of mirror pairs. The reflectivity factor *r* for a DBR with *m* mirror pairs is given by

$$r = \frac{n_0 - (n_{\mathrm{AlAs}}/n_{\mathrm{GaAs}})^{2m}}{n_0 + (n_{\mathrm{AlAs}}/n_{\mathrm{GaAs}})^{2m}} \tag{21}$$

with $n_0 = 1$ for the bottom and $n_0 = n_{\mathrm{GaAs}}$ for the top mirror, respectively.

By using 20/23 (24/27) top/bottom mirror pairs for the MC1 (MC2) design, $n_{\mathrm{GaAs}} = 3.544$, $n_{\mathrm{AlAs}} = 2.973$, $d_{\mathrm{GaAs}} + d_{\mathrm{AlAs}} = 150$ (142) nm, $d_{\mathrm{cav}} = 270$ (260) nm and $\lambda = 960$ (940) nm an effective cavity length of 6.49 μm (6.16 μm) and a *Q*-factor of 45 400 (126 000) can be calculated [30]. In figure 11, a cross section of the MC2 design is shown. The structure is grown by molecular beam epitaxy (MBE) and consists of AlAs/GaAs Bragg mirrors grown at 590 °C. The embedded $Ga_{0.7}In_{0.3}As$ layer is grown at 510 °C and is comparable to the elongated dot structure shown in figure 5(*c*). The position of the single dot layer is at the anti-node of the vertically confined field distribution.

The reflectance spectrum of the planar structure is plotted in figure 12. The stop band is well pronounced and the dip

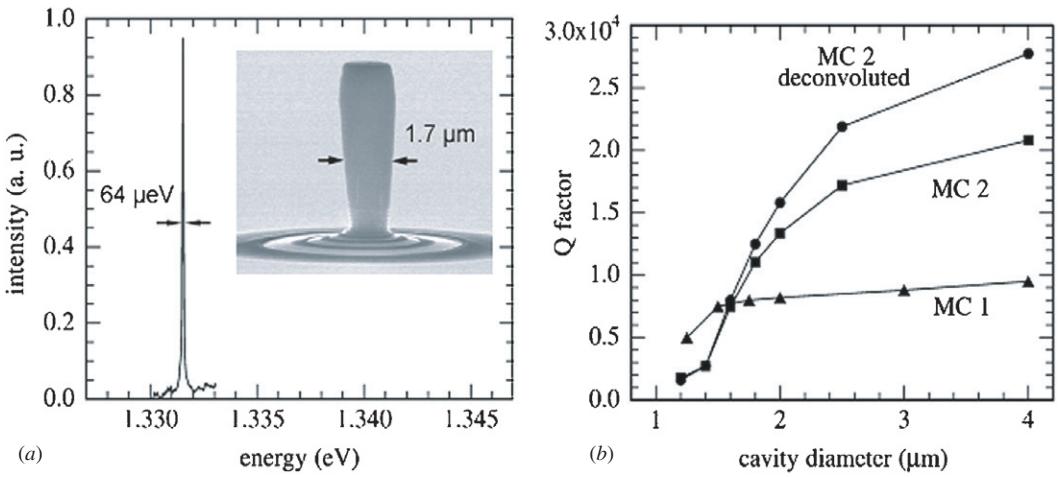

Figure 13. (*a*) The PL emission spectrum of a 4 μm wide micropillar cavity exhibiting a Q-factor of about 20 000. The inset shows micropillar cavity with a nominal diameter of 2 μm and an etch depth of about 6 μm. The arrows indicate the position of the dot layer and the real diameter, (*b*) dependence of the Q-factor from the cavity diameter for two different Bragg resonator designs consisting of 20/23 (MC1) and 24/27 (MC2) top/bottom mirrors, respectively. The dots show the deconvoluted values of MC2 by taking into account the finite spectrometer resolution. From [30].

near 950 nm indicates the position of the cavity resonance. The dot structure is designed in such a way that there is a weak spectral overlap only with the largest dots, i.e., with the low-energy part of the spectrum, as can be seen from the PL spectrum in figure 12. This allows the coupling of single dots with the cavity resonance.

The micropillar fabrication is performed by electron beam lithography and dry-etching by using a metal etch mask for deep etching. Details of the process are described in [30]. In figure 13(*a*), a micropillar structure with a nominal diameter of 2 μm and an etch depth of 6 μm is shown. Due to underetching and mask erosion the cross section shows slightly tilted side-walls. For larger diameters, this underetch effect is less severe and a Q-factor of more than 20 000 could be obtained for a pillar diameter of 4 μm. In figure 13(*b*), the Q-factor is plotted as function of the pillar diameter for the above discussed two different Bragg resonator designs MC1 and MC2. By taking into account the limited spectral resolution of the used spectrometer, a deconvoluted Q-factor of about 28 000 could be determined at the largest realized pillar diameter.

However, the Q-factor degrades significantly for smaller pillar diameters. Therefore, there is a trade-off between small mode volume and high Q-factors according to equation (19). The mode volume for pillars is proportional to the square of the pillar diameter d_c. In figure 14, Q/d_c is plotted as a function of the pillar diameter for the MC1 design. Although the Q-factor decreases at a pillar diameter of 1.5 μm to already 8000, the figure of merit for strong coupling has its maximum, which makes the smaller pillars more suitable for strong coupling experiments. With such structures, strong coupling effects could be already demonstrated [6].

If one compares the experimentally achieved Q-values with the theoretically predicted values by equation (20), the potential of the planar cavities could be only partially utilized although the trend is visible going from MC1 to MC2 design. However, especially due to the limited sidewall quality this advantage of mirror reflectivities cannot be utilized at smaller

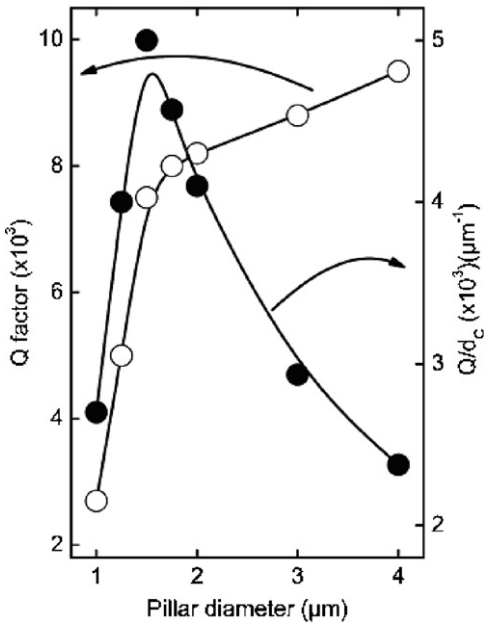

Figure 14. The Q-factor (open dots) and Q/d_c (filled dots) as a function of the pillar diameter for a MC1 design. From [57].

pillar diameters. In addition, at higher Q-factors residual absorption and side-wall roughness scattering limits also the Q-factor at larger pillar diameters.

To improve the microcavity quality, the etch process was further optimized. In the inset of figure 15, a micropillar with nearly perfect rectangular sidewalls is shown using an optimized ECR-RIE process [58]. Due to the reduced sidewall roughness, the Q-factor could be improved to 165 000 at 4 μm pillar diameter and more than 40 000 for $d_c = 1.7$ μm. Therefore the Q-factor could be increased by a factor of 5 and the figure of merit for strong coupling by a factor of 4.4. In figure 15(*b*), the PL spectrum of a 4 μm micropillar is shown with a linewidth of 9.6 μeV (see the inset) and a large mode splitting to the next circular mode triplet.

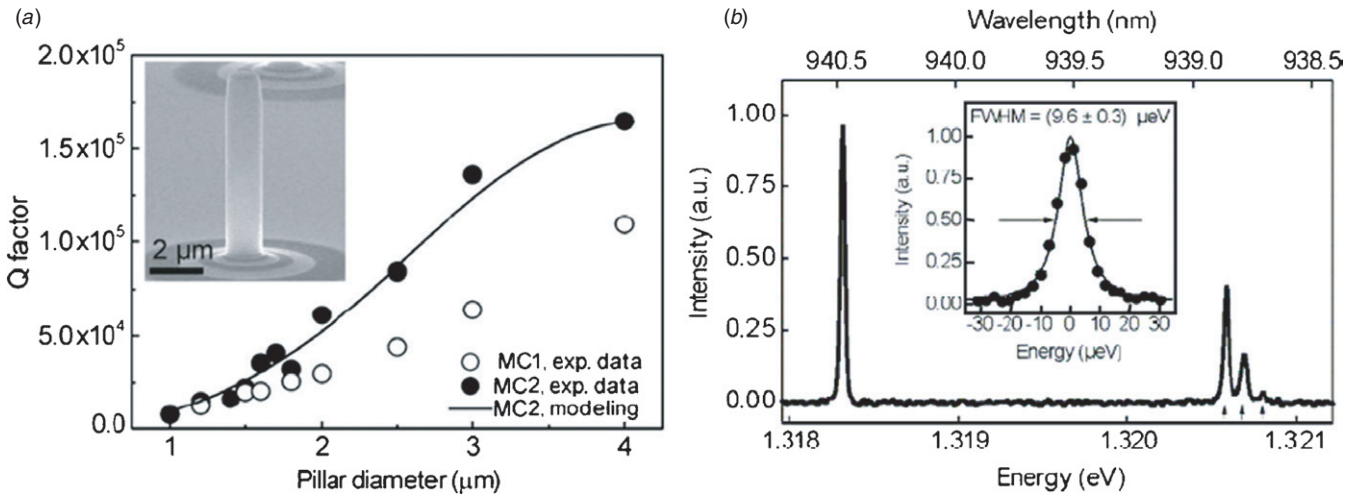

Figure 15. (*a*) The *Q*-factor of micropillars with an improved etched process as a function of the pillar diameter. The inset shows a SEM picture of a 2 μm pillar, (*b*) low temperature PL spectrum of a 4 μm micropillar. The inset shows a highly resolved spectrum of the fundamental mode. The arrows indicate the calculated mode positions of the next higher circular mode triplet. (Reprinted with permission from [58] copyright 2007 American Institute of Physics.)

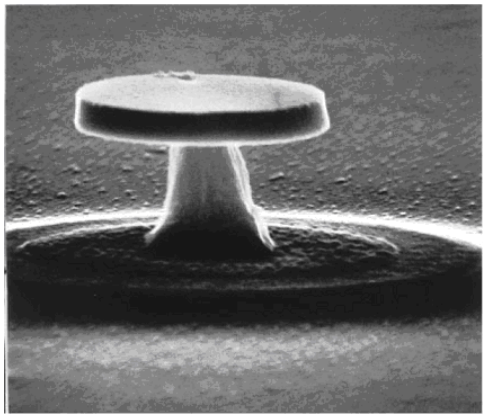

Figure 16. SEM picture of a GaAs microdisc cavity with 2 μm diameter. (Reprinted with permission from [61] copyright 1999 American Institute of Physics.)

The advantage of high-*Q* micropillars is the efficient vertical outcoupling geometry, which will allow an easy fibre coupling, e.g., for single photon sources. The *Q*-values in the mean-time are much higher than needed for strong coupling, which gives already a larger margin in the design of the interacting dot structures, e.g., strong coupling is now also possible with smaller dots. Due to the larger mode volume of micropillars, the positioning accuracy is about 100 nm more relaxed in comparison to PC cavities. On the other hand, the coupling in integrated photonic circuits, just as it is easily possible with PC cavities, is more sophisticated and will be very limited.

3.2.3. Microdisc cavities. With microdisc structures ultra-high *Q*-values were achieved in silicon on insulator discs with *Q*-values up to 3 million [60]. However, with a disc diameter of 40 μm the mode volume is relatively large and to combine the silicon technology with optically active materials is difficult.

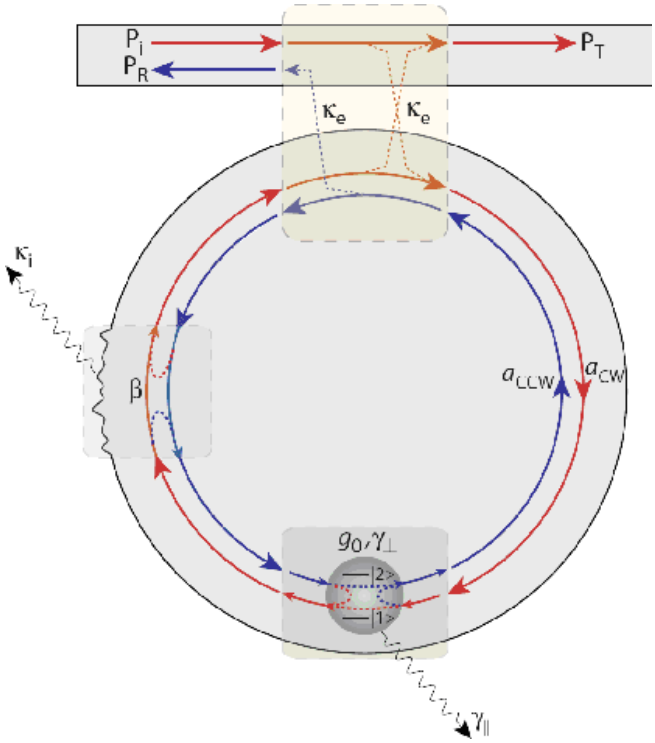

Figure 17. Coupling scheme of a microdisc with a weakly coupled waveguide. Due to surface imperfections energy splitted modes are present (ccw = counter clockwise, cw = clockwise). The dot is coupled with one of those modes. (Reprinted with permission from [62] copyright 2007 American Physical Society.)

For GaAs based microdisc structures the vertical confinement has to be realized with a free-standing disc due to the lack of a high-quality oxide. In figure 16, a GaAs microdisc standing on a post is shown with a disc diameter of 2 μm [61]. The disc is fabricated by MBE on a GaAs/AlGaAs heterostructure. After a GaAs buffer, a 1 μm thick $Al_{0.8}Ga_{0.2}As$ layer is grown by MBE, which serves as a sacrificial layer. The 200 nm thick

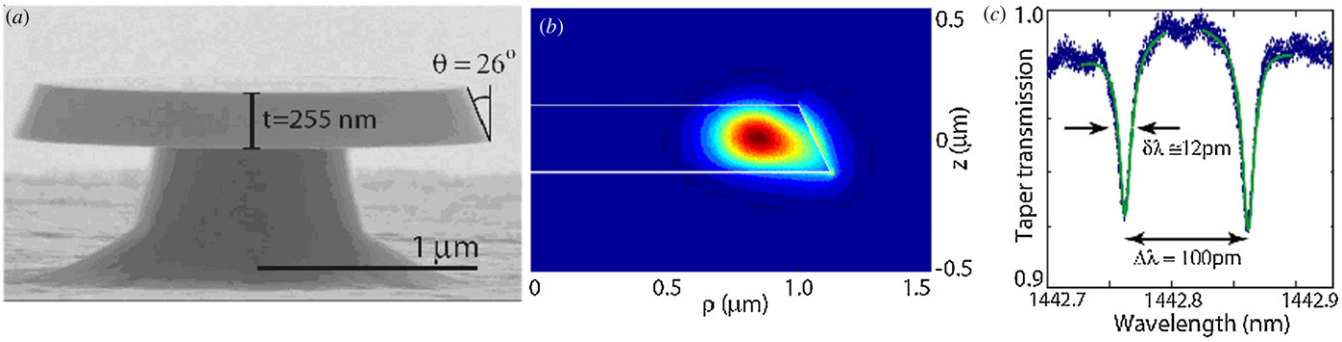

Figure 18. (*a*) SEM picture of a 2.12 μm GaAs microdisc, (*b*) the calculated vertical mode profile and (*c*) Waveguide modes for ccw and cw modes. (Reprinted with permission from [62] copyright 2007 American Physical Society.)

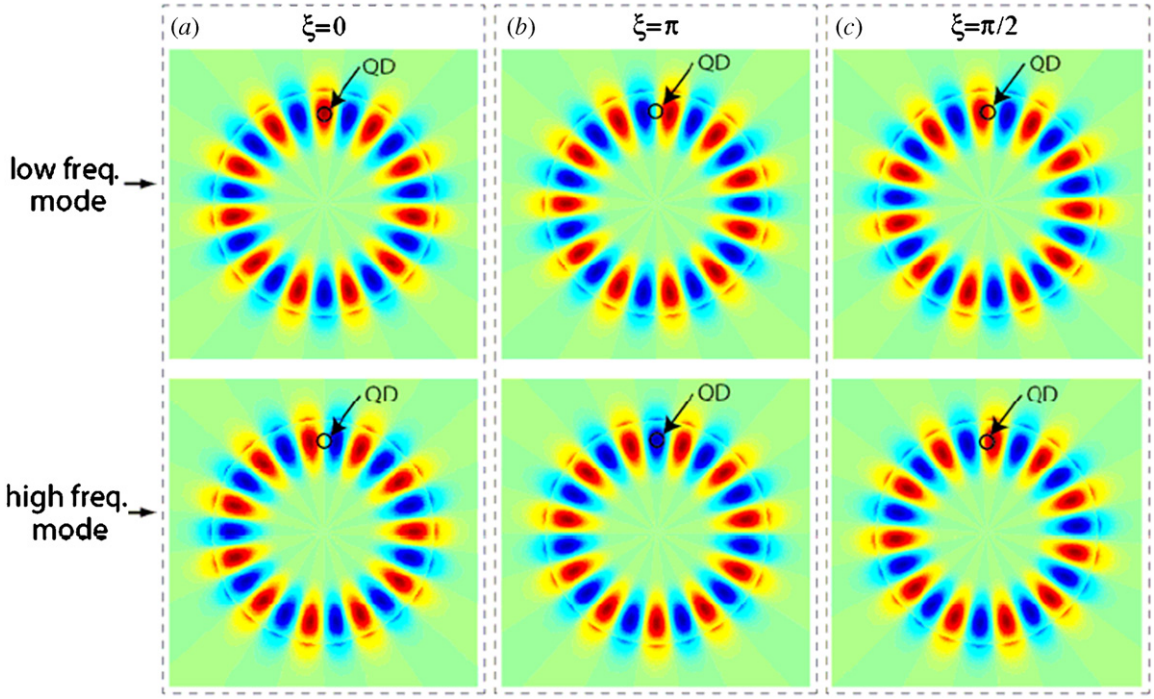

Figure 19. Standing waves (low- and high-frequency modes) in a microdisc with different phases. A fixed QD position is assumed as indicated. (Reprinted with permission from [62] copyright 2007 American Physical Society.)

GaAs disc layer is embedded by 25 nm thick $Al_{0.4}Ga_{0.6}As$ optical confinement layers on both sides. The structure is capped by 2 nm GaAs. Centred in the microdisc layer two high-density InAs QD layers are included. The disc structure is first dry-etched down to the GaAs buffer layer and the sacrificial layer is subsequently removed by diluted HF until only a post remains.

With these structures *Q*-factors of 12 000 were obtained but the threshold for strong coupling could not be achieved with a standard QD.

A different microdisc approach was developed by Peter *et al* [8] by using QDs based on interface fluctuations. With these dots, which allow still a confinement potential for excitons of about 15 meV, a much larger dipole moment than for self-assembled InAs dots could be obtained resulting in the observation of strong coupling phenomena also in microdiscs.

A detailed description about microdisc specific phenomena is reported by Srinivasan and Painter [62]. In figure 17, the considered coupling scheme is illustrated. The weakly coupled waveguide serves as a read-out for the whispering gallery modes in the disc without significantly influencing the mode properties. Due to surface imperfections two modes exist, i.e., a counter clockwise mode and a clockwise mode, with slightly different resonance energies.

In figure 18(*a*), a fabricated microdisc structure is shown with a diameter of 2.12 μm and a slab thickness of 255 nm. In figure 18(*b*), the simulated mode profile is shown, while in figure 18(*c*), the mode spectrum of the two modes are plotted with a wavelength split of 0.1 nm.

In figure 19, the lateral mode profiles of low- and high-frequency modes of a microdisc is shown for different phases, which lead to different overlaps with the quantum dot for the two different modes. Due to the higher overlap with the low-

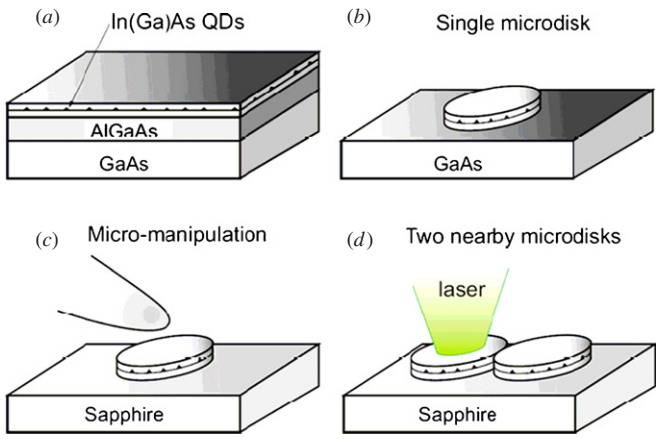

Figure 20. Schematic illustration of the fabrication and manipulation methods for GaAs microdiscs containing (Ga,In)As dots. (Reprinted with permission from [65] copyright 2008 American Physical Society.)

frequency mode, one should only expect Rabi oscillations with that mode.

The problem of accurate spatial and spectral alignment of QDs in microdiscs is quite similar to the PC cavities. An interesting approach for spectral alignment is laser heating as shown by Rastelli *et al*, [63] which allows a fine tuning of the exciton transition after device processing. In addition, the dot position could be controlled by pre-patterning of surfaces prior to the dot growth [64].

A proposal for the planar integration of microdiscs is shown by Benyoucef *et al* [65]. In figure 20, the fabrication technique is described starting from the epitaxy (a), free-etching of discs (b), micromanipulation onto a Sapphire substrate (c) and mode alignment by local laser heating (d). By strong coupling of the disc modes, also longer distances can be reached without loosing the phase correlation.

Also other geometries can be used to favourize whispering-gallery modes, as in high-quality micropillars, as was reported by two groups [66, 67].

4. Optical experiments within the strong coupling regime

4.1. Quantum dots in microcavity pillars

The investigations of strong coupling effects between quantum dots and cavity modes is mainly performed by low-temperature highly spatially resolved photoluminescence spectroscopy. As a major variation parameter the temperature is tuned to test the behaviour at the cross-over point. Due to the different temperature dependence of the transition energy of the exciton and the cavity resonance energy the energetic overlap between the two peaks can be controlled. While the exciton transition follows mainly the bandgap change, the cavity resonance changes only due to the temperature dependence of the refractive index, which is about a factor of 5 weaker than the bandgap change. This behaviour is the same for all three considered cavity structures of figure 8.

As a criterion for strong coupling, the anti-crossing behaviour at the cross-over point of the two peaks will be used. In the case of coherent coupling of the two modes a polariton state is created with two splitted peaks. The peak distance is identical to the Rabi oscillation frequency as determined by equation (16). For comparison to the strong coupling case also the case of weak coupling is shown in figure 21 [6, 68]. The bold highlighted spectrum in figure 21(*b*) is precisely at the cross-over point. Here, no peak splitting can be observed but a strong intensity enhancement and a linewidth, which is narrower than the cavity resonance can be verified as expected by theory. By a slight increase of the Q-factor and may be also by a better spatial overlap of the QD with the cavity mode an anti-crossing behaviour can be observed as shown in figure 21(*a*).

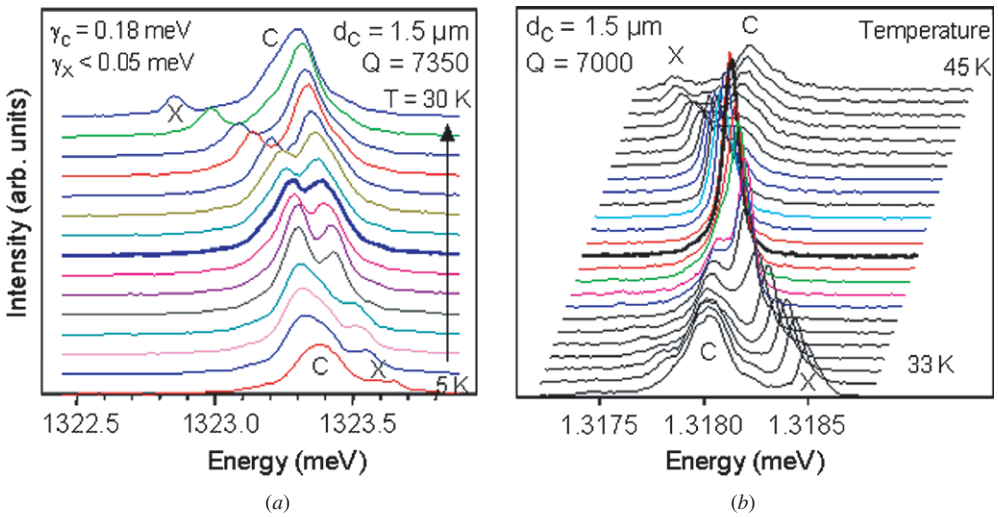

Figure 21. PL spectra from a micropillar cavity in the strong (*a*) and weak (*b*) coupling regime. The sample temperature is indicated. X and C denote exciton and cavity lines, respectively. From [6].

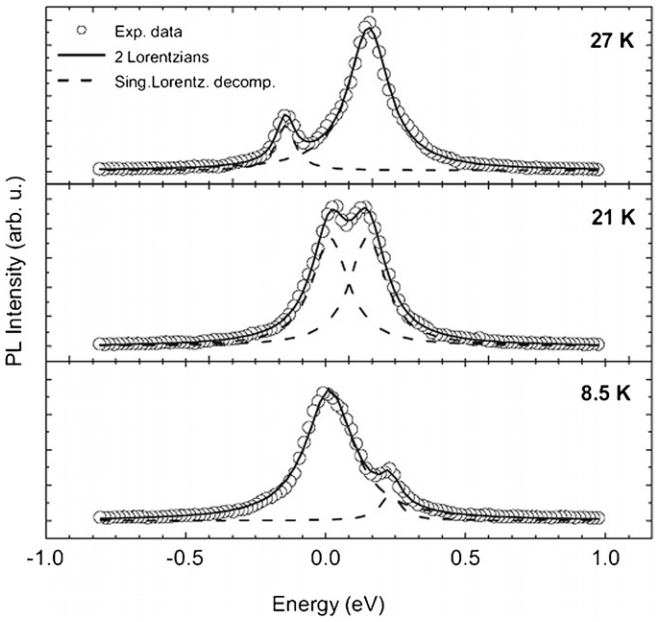

Figure 22. PL spectra at three different temperatures of a micropillar structure in the strong coupling regime near or at the cross-over point (cf figure 21(*b*)). The solid and dashed lines indicate peak fits. From [68].

In figure 22, PL spectra at and near the cross-over point are shown with high spectral resolution. The peak fits at 21 K (solid and dashed lines) show clearly the identical peak properties, i.e., peak intensity and linewidth, of the two polariton modes. As expected, the peaks can be fitted by Lorentzian functions.

In figure 23, the peak energy, linewidth and intensity of the same micropillar structure are shown as function of the detuning energy in the strong (*a*) and weak (*b*) coupling regime. Here, the anti-crossing and crossing behaviour in the strong and weak-coupling case, respectively, is clearly visible as well as the strong differences in the linewidth and intensity behaviour. In the weak-coupling case, the resonance enhancement is about a factor of 3.

Due to the large mode volume in micropillars ($d_c > 1\ \mu$m) the probability in medium dense QD layers is high that more than 1 QD is within the temperature tuning range. With some luck, it is even possible to find some situations, where more than one QD are in resonance with the cavity mode and can be coherently coupled via the light field [69]. This situation is illustrated in figure 24 for a micropillar cavity with a diameter of 1.6 μm and a Q-factor of 9500.

In figure 25, peak positions are plotted against the detuning energy in the case of strong coupling of two QDs at the same time (top) and subsequently (bottom). Here clearly the anti-crossing behaviour of all three lines can be observed resulting in the case of simultaneous coupling of 2 QDs to a triplet peak structure, which proves the coherent coupling of two individual excitons with the light field. In the second case, the spectral distance of the two exciton transitions is too large and only subsequent strong coupling could be obtained.

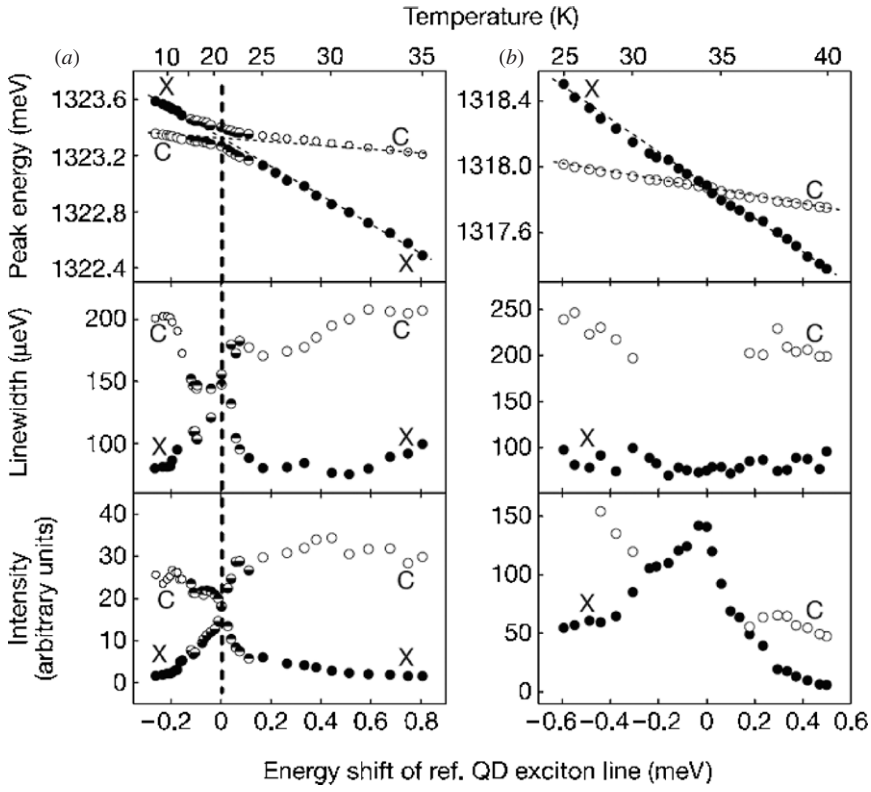

Figure 23. Peak energy, linewidth and intensity as a function of the detuning energy controlled by sample temperature in the strong (*a*) and weak (*b*) coupling regime. From [6].

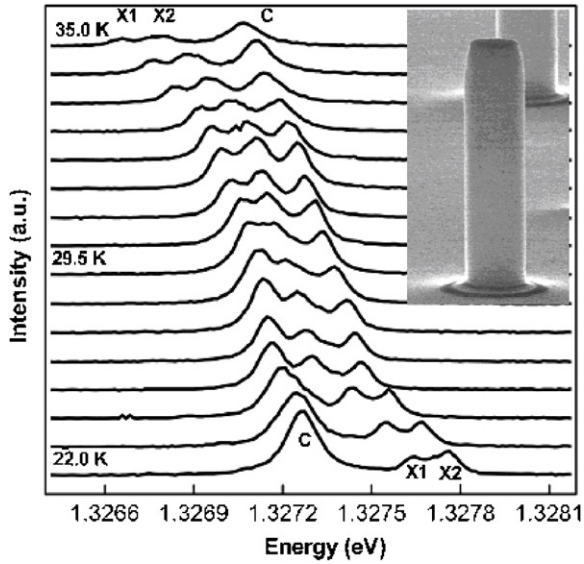

Figure 24. PL spectra of a micropillar structure of 1.6 μm in diameter with a Q-factor of 9500 for different temperatures. Here two individual QDs are in resonance resulting in a peak splitting of 120 μeV. The inset shows a SEM picture of such a structure. From [69].

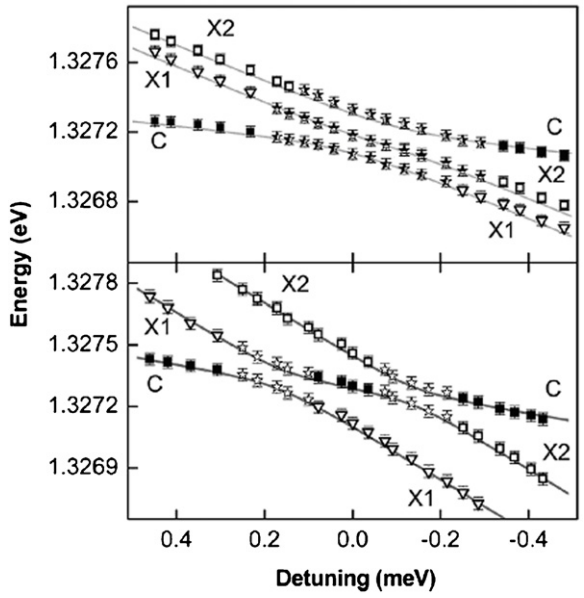

Figure 25. Peak positions as a function of the detuning energy in the case of simultaneous strong coupling of two QDs (top) and subsequent strong coupling of QDs (bottom). From [69].

This experiment shows the potential of high-Q micropillar cavities to couple coherently more than one dot. With structures of higher Q-values, as already shown in section 3.2 and position controlled QDs, one should be able to scale it further up to several QDs.

To prove that the observed strong coupling phenomena are related to single photon interactions, correlation measurements were performed on micropillar structures [70]. In figure 26, different correlation functions are plotted. In (a) the autocorrelation function at resonance condition shows a low

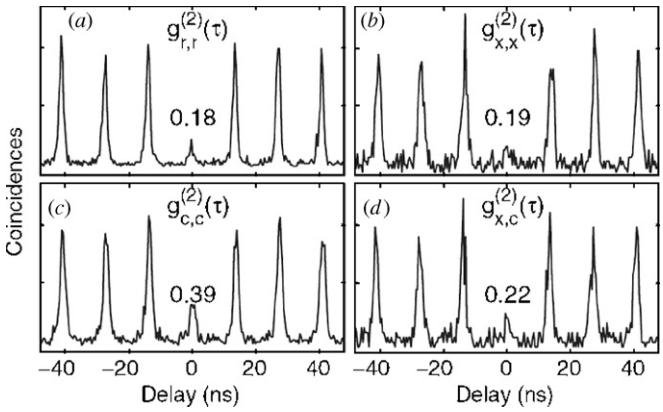

Figure 26. Correlation functions for different conditions. (*a*) Autocorrelation in resonance condition, (*b*) autocorrelation of exciton emission in case of 0.4 nm detuning from cavity resonance, (*c*) autocorrelation of cavity resonance emission and (*d*) cross-correlation between exciton and cavity resonance emission. (Reprinted with permission from [70] copyright 2007 American Physical Society.)

probability of two photon events of 0.18 (<0.5), which proves the dominant single particle interaction in these cavities. By detuning the system of about 0.4 nm in peak distance between exciton and cavity peak, the system is tested as well. The autocorrelation function of exciton emission shows nearly no two-photon events, i.e., as expected, there is only one exciton excited at the same time. Surprisingly, also the autocorrelation of the cavity emission shows a low correlation value, which indicates that the photon source is mainly related to the exciton transition. This is directly proven by the cross-correlation between cavity and exciton peaks and shows that the photon source has the same origin.

4.2. Quantum dots in microdiscs and photonic crystal cavities

By Yoshie *et al*, [7] strong coupling was the first time obtained in a photonic crystal cavity using the *L*3 geometry as illustrated in figure 9(*a*). In figure 27, the temperature tuned spectra near the cross-over point is shown with a clear double peak spectrum. Figure 27(*c*) shows the anti-crossing behaviour as a function of the wavelength over a wider temperature tuning range. With a Q-factor of 13 300 a Rabi splitting energy of 170 μeV can be observed.

By Hennessy *et al* [46] similar optical spectra could be determined for a pre-positioned QD structure with a QD stack for surface marking (cf figure 10). In figure 28, the wavelength shift of the polariton peaks and corresponding spectra are shown as function of the detuning. The detuning is performed here by monolayer deposition [71]. However, in contrast to the previous experiments, they observed a triple peak at resonance position, which could not be fully clarified yet. One possible explanation is the contribution of some incoherent light, which is weakly coupled to the cavity resonance.

An indication that a significant contribution of incoherent light can be the origin of the central peak gives autocorrelation measurements as shown in figures 29(*c*) and (*d*). Although

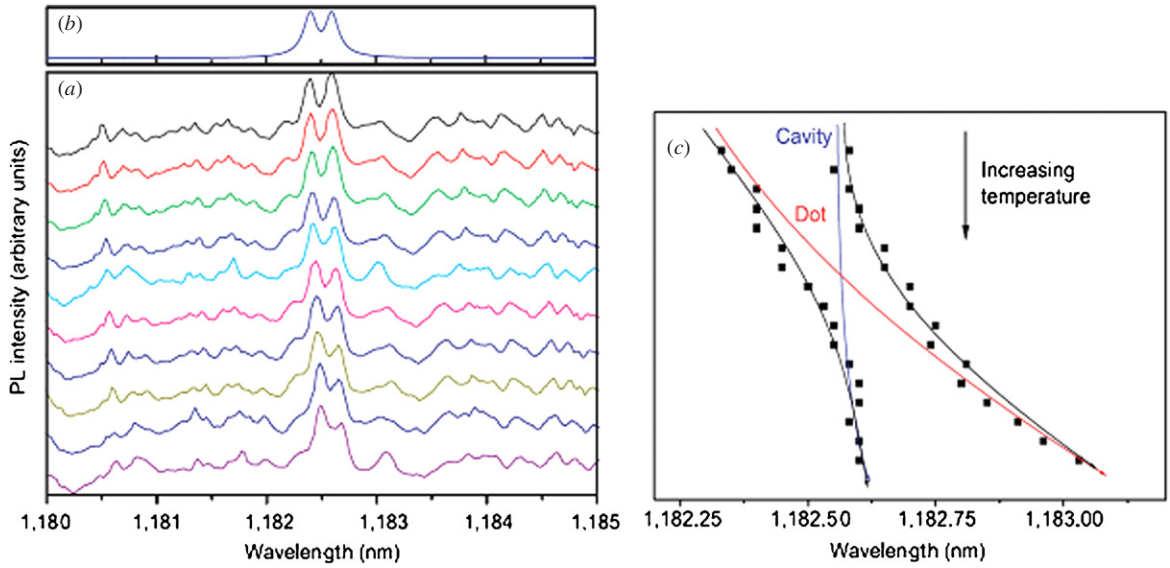

Figure 27. (*a*) PL spectra recorded at different temperatures in steps of 0.5 K, (*b*) Simulated double-peak spectrum assuming uncoupled individual linewidths of $\gamma_C = 0.2$ nm and $\gamma_X = 0.1$ nm and (*c*) temperature dependence of the emission wavelengths of the two peaks showing anti-crossing behaviour. (Reprinted with permission from [7] copyright 2004 Macmillan Publishers Ltd.)

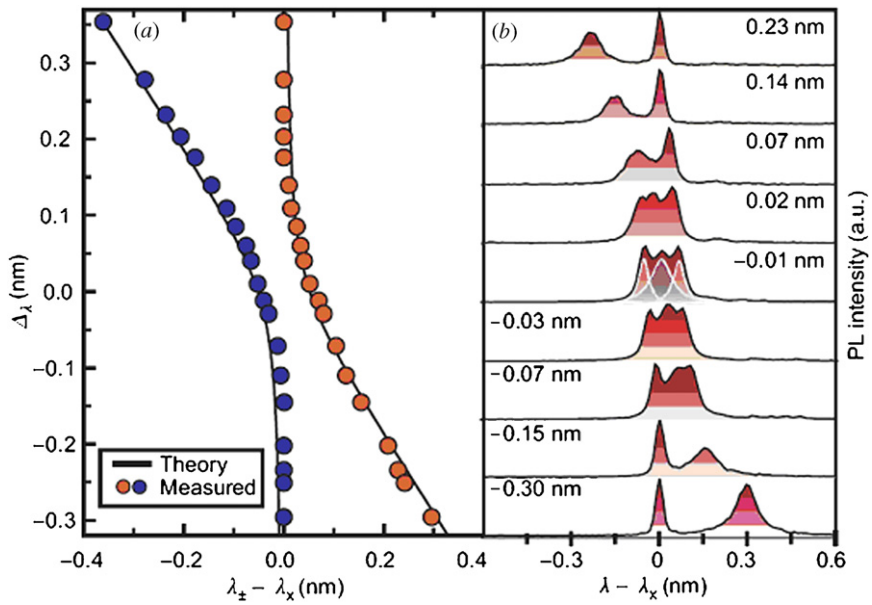

Figure 28. (*a*) Wavelength shift of the two polariton peaks as a function of the detuning. (*b*) PL spectra for different detuning wavelengths. (Reprinted with permission from [46] copyright 2007 Macmillan Publishers Ltd.)

a clear quantum correlation effect can be observed, the signal has a large background of un-correlated events.

In this work also the inhibition and enhancement of spontaneous light emission in off- and on-resonance condition can be clearly observed, which results in an increased exciton lifetime of 8.7 ns at 4.1 nm detuning and a strong lifetime reduction to 60 ps in resonance [46]. In comparison, the exciton lifetime is about 1 ns in QD material without cavity structure. In this experiment the increase in spontaneous lifetime is more pronounced than in previous experiments, [72] but this is no specific signature for strong coupling as stated by the authors. A strong enhancement occurs also at the weak-coupling regime.

Finally, the strong coupling results from Peters *et al* [8] are highlighted in figure 30. They used a microdisc structure as shown in figure 16. Although the individual linewidths are in the range of 200 μeV, the peak separation is very pronounced and reached a record value of 400 μeV. This value is also consistent with the large oscillator strength of interfacial dots and the small mode volume of whispering gallery modes.

5. Conclusions and outlook

Although it took quite some effort and time to obtain strong coupling effects in semiconductor quantum dot systems, i.e., to realize a coherent coupling between single particles like

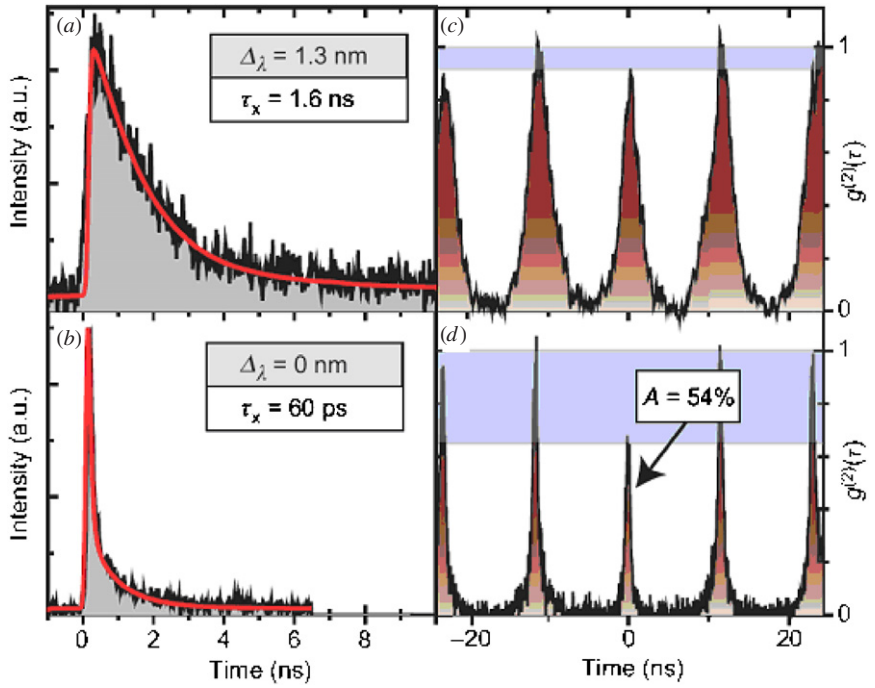

Figure 29. (*a*) and (*b*) Time resolved measurements at 1.3 and 0 nm detuning, (*c*) the autocorrelation function of the cavity mode in off-resonance condition showing no quantum correlation and (*d*) the autocorrelation function of the cavity mode in on-resonance condition showing strong quantum correlation but with some uncorrelated background. (Reprinted with permission from [46] copyright 2007 Macmillan Publishers Ltd.)

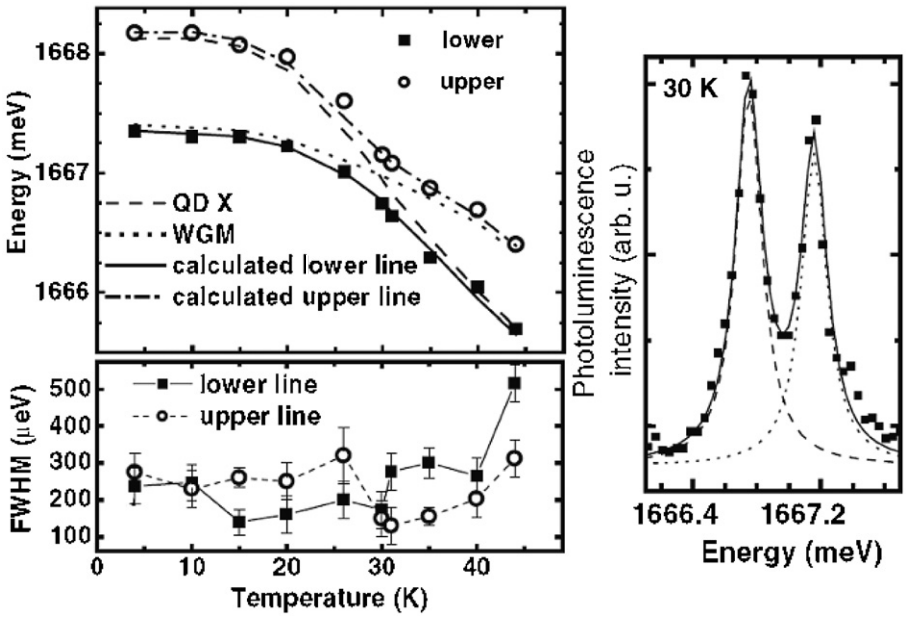

Figure 30. Energies and linewidth of polariton peaks as a function of temperature in the case of a microdisc structure (left). PL spectrum in resonance condition (right). (Reprinted with permission from [8] copyright 2005 American Physical Society.)

exciton and photon, well-established technologies are now available, which allow predictable properties with different fabrication technologies and structure designs. In this paper a review was given about mainly three approaches to realize high-Q cavities for strong quantum dot interactions with photons, i.e., photonic crystal membrane cavities, micropillar and microdisc cavities. In all three cases strong coupling effects could be obtained. In the meantime further progress is made in the fabrication technology by controlling the dot position relative to the mode profile to achieve optimum coupling properties and post-fabrication fine tuning of cavities by monolayer oxidation or deposition. Also the first experiment of strong coupling of spatially separated QDs

opens the potential to further scale up the systems to more complex structures.

The work on cavity-enhanced light–matter interactions opens the field of optoelectronics down to the single particle level and quantum systems. It is very fascinating here that it will be possible in the near future that the local quantum information of electronic states can be transferred over large distances to entangle different electronic states at different locations, e.g., in photonic crystal based integrated photonic circuits. Still an open point will be here to adjust the energetic position of individual dots. But techniques like laser annealing could address this already.

Although there is still a long way to go for the realization of quantum processors, the cavity-enhanced strong coupling effects have the potential to supply key functionalities necessary for semiconductor-based systems and which allow an easy access to the macroscopic world via optical interfaces.

Applications which may be nearer in the future are single photon sources with enhanced single photon yield for quantum cryptography [73, 74] and ultra-miniaturized lasers for on-chip light generation. The latter gain here on the possibility of realizing threshold-less lasers due to the high spontaneous coupling factor [75, 76].

Acknowledgments

The financial support of a part of the work by the EU project 'QPhoton' as well as the comments and corrections received by Gadi Eisenstein (Technion) and Alfredo di Rossi (Thales R&T) is highly acknowledged.

References

[1] Walther H 2001 Laser experiments with single atoms and the test of basic quantum phenomena *Opt. Spectrosc.* **91** 327
[2] Haroche S and Kleppner D 1989 Cavity quantum electrodynamics *Phys. Today* **42** 24
[3] Berman P 1994 *Cavity Quantum Electrodynamics* (San Diego, CA: Academic)
[4] Weisbuch C and Rarity J 1996 *Microcavities and Photonic Bandgaps: Physics and Applications (NATO ASI Series E324)* (Dordrecht: Kluwer)
[5] Boca A, Miller R, Birnbaum K M, Boozer A D, McKeever J and Kimble H J 2004 Observation of the vacuum Rabi spectrum for one trapped atom *Phys. Rev. Lett.* **93** 233603
[6] Reithmaier J P, Sęk G, Löffler A, Hofmann C, Kuhn S, Reitzenstein S, Keldysh L, Kulakovskii V, Reinecke T L and Forchel A 2004 Strong coupling in a quantum dot micropillar cavity system *Nature* **432** 197
[7] Yoshie T, Scherer A, Hendrickson J, Khitrova G, Gibbs H M, Rupper G, Ell C, Shekin O B and Deppe D G 2004 Vacuum Rabi splitting with a single quantum dot in a photonic crystal nanocavity *Nature* **432** 200
[8] Peter E, Senellart P, Martrou D, Lemaître A, Hours J, Gérard J M and Bloch J 2005 Exciton-photon strong-coupling regime for a single quantum dot embedded in a microcavity *Phys. Rev. Lett.* **95** 067401
[9] Khitrova G, Gibbs H M, Kira M, Koch S W and Scherer A 2006 Vacuum Rabi splitting in semiconductors *Nature Phys.* **2** 81
[10] Reithmaier J P, Röhner M, Zull H, Schäfer F and Forchel A 1997 Size dependence of confined optical modes in photonic quantum dots *Phys. Rev. Lett.* **78** 378
[11] Gérard J M, Sermage B, Gayral B, Legrand B, Costard E and Thierry-Mieg V 1998 Enhanced spontaneous emission by quantum boxes in a monolithic optical microcavity *Phys. Rev. Lett.* **81** 1110
[12] Bayer M, Reinecke T L, Weidner F, Larionov A, McDonald A and Forchel A 2001 Inhibition and enhancement of the spontaneous emission of quantum dots in structured microresonators *Phys. Rev. Lett.* **86** 3168
[13] Solomon G S, Pelton M and Yamamoto Y 2001 Single-mode spontaneous emission from a single quantum dot in a three-dimensional microcavity *Phys. Rev. Lett.* **86** 3903
[14] Khitrova G, Gibbs H, Jahnke F, Kira M and Koch S 1999 Nonlinear optics of normal-mode-coupling semiconductor microcavities *Rev. Mod. Phys.* **71** 1591
[15] Rudin S and Reinecke T L 1999 Oscillator model for vacuum Rabi splitting in microcavities *Phys. Rev.* B **59** 10227
[16] Adreani L, Panzarini G and Gérard J M 1999 Strong-coupling regime for quantum boxes in pillar microcavities: theory *Phys. Rev.* B **60** 13276
[17] Purcell E M 1946 Spontaneous emission probabilities at radio frequencies *Phys. Rev.* **69** 681
[18] Zrenner A, Butov L V, Hagn M, Abstreiter G, Böhm G and Weimann G 1994 Quantum dots formed by interface fluctuations in AlAs/GaAs coupled quantum well structures *Phys. Rev. Lett.* **72** 3382
[19] Brunner K, Abstreiter G, Böhm G, Tränkle G and Weimann G 1994 Sharp line photoluminescence and two photon absorption of zero-dimensional bi-excitons in a GaAs/AlGaAs structure *Phys. Rev. Lett.* **73** 1138
[20] Gammon D, Snow E S, Shanabrook B V, Katzer D S and Park D 1996 Fine structure splitting in the optical spectra of single GaAs quantum dots *Phys. Rev. Lett.* **76** 3005
[21] von Freymann G *et al* 2002 Level repulsion in nano-photoluminescence spectra from single GaAs quantum wells *Phys. Rev.* B **65** 205327
[22] Marzin J Y, Gérard J M, Izrael A, Barrier D and Bastard G 1994 Photoliminescence of single InAs quantum dots obtained by self-organized growth on GaAs *Phys. Rev. Lett.* **73** 716
[23] Leonard D, Krishnamurthy M, Reaves C M, Denbaars S P and Petroff P M 1993 Direct formation of quantum-sized dots from uniform coherent islands of InGaAs on GaAs surfaces *Appl. Phys. Lett.* **63** 3203
[24] Moison J M, Houzay F, Barthe F, Leprince L, André E and Vatel O 1994 Self-organized growth of regular nanometer-scale InAs dots on GaAs *Appl. Phys. Lett.* **64** 196
[25] Petroff P M, Lorke A and Imamoglu A 2001 Epitaxially self-assembled quantum dots *Phys. Today* **54** 46
[26] Bimberg D, Grundmann M and Ledentsov N N 1999 *Quantum Dot Heterostructures* (New York: Wiley)
[27] Reithmaier J P and Forchel A 2003 Recent advances in semiconductor quantum dots lasers *Comptes Rendus Physique* **4** 611
[28] Reithmaier J P *et al* 2005 InP based lasers and optical amplifiers with wire-/dot-like active regions (invited review paper) *J. Phys.* D **38** 2088
[29] Reithmaier J P *et al* 2006 Semiconductor quantum dots devices: recent advances and application prospects *Phys. Status Solidi* b **243** 3981–7
[30] Löffler A, Reithmaier J P, Sęk G, Hofmann C, Reitzenstein S, Kamp M and Forchel A 2005 Semiconductor quantum dot microcavity pillars with high quality factors and enlarged dot dimensions *Appl. Phys. Lett.* **86** 111105
[31] Löffler A, Reithmaier J P, Forchel A, Sauerwald A, Peskes D, Kümmell T and Bacher G 2006 Influence of the strain on the formation of GaInAs/GaAs quantum structures *J. Cryst. Growth* **286** 6–10

[32] Löffler A, Poloczek P, Sęk G, Misiewicz J, Reithmaier J P and Forchel A 2006 Optical characteristics of lowly strained GaInAs quantum dots *Phys. Status Solidi* c **3** 3815–8
[33] Sek G, Poloczek P, Ryczko K, Misiewicz J, Löffler A, Reithmaier J P and Forchel A 2006 Photoreflectance determination of the wetting layer thickness in the $In_xGa_{1-x}As/GaAs$ quantum dot system for a broad indium content range of 0.3–1 *J. Appl. Phys.* **100** 103529
[34] Yablonovitch E 1987 Inhibited spontaneous emission in solid-state physics and electronics *Phys. Rev. Lett.* **58** 2059
[35] John S 1987 Strong localization of photons in certain disordered dielectric superlattices *Phys. Rev. Lett.* **58** 2486
[36] Gourley P L, Wendt J R, Vawter G A, Brennan T M and Hammons B E 1994 Optical properties of two-dimensional photonic lattices fabricated as honeycomb nanostructures in compound semiconductors *Appl. Phys. Lett.* **64** 687
[37] Fan S H, Villeneuve P R, Joannopoulos J D and Schubert E F 1997 High extraction efficiency of spontaneous emission from slabs of photonic crystals *Phys. Rev. Lett.* **78** 3294
[38] Painter O, Lee R K and Scherer A 1999 Two dimensional photonic band-gap defect mode laser *Science* **284** 1819
[39] Srinivasan K, Barclay P E, Painter O, Chen J X, Cho A Y and Gmachl C 2003 Experimental demonstration of a high quality factor photonic crystal microcavity *Appl. Phys. Lett.* **83** 1915
[40] Akahane Y, Asano T, Song B S and Noda S 2003 High-Q photonic nanocavity in a two dimensional photonic crystal *Nature* **425** 944
[41] Song B S, Noda S, Asano T and Akahane Y 2005 Ultra-high Q photonic double-heterostructure nanocavity *Nature Mater.* **4** 207
[42] Takahashi Y, Hagino H, Tanaka Y, Song B S, Asano T and Noda S 2007 High-Q nanocavity with a 2-ns photon lifetime *Opt. Express* **15** 17206
[43] Weidner E, Combrié S, Tran N V Q, De Rossi A, Nagle J, Cassette S, Talneau A and Benisty H 2006 Achievement of ultrahigh quality factors in GaAs photonic crystal membrane nanocavity *Appl. Phys. Lett.* **89** 221104
[44] Noda S, Fujita M and Asano T 2007 Spontaneous-emission control by photonic crystals and nanocavities *Nature Photon.* **1** 449
[45] Bandolato A, Hennessy K, Atatüre M, Dreiser J, Hu E, Petroff P M and Imamoglu A 2005 Deterministic coupling of single quantum dots to single nanocavity modes *Science* **308** 1158
[46] Hennessy K, Badolato A, Winger M, Gerace D, Atatüre M, Gulde S, Fält S, Hu E L and Imamoglu A 2007 Quantum nature of a strongly coupled single quantum dot-cavity system *Nature* **445** 896
[47] DeSalvo G C *et al* 1996 Wet chemical digital etching of GaAs at room temperature *J. Electrochem. Soc.* **143** 3652
[48] Mosor S, Hendrickson J, Richards B C, Weet J, Khitrova G, Gibbs H M, Yoshie T, Scherer A, Shckekin O B and Deppe D G 2005 Scanning a photonic crystal slab nanocavity by condensation of xenon *Appl. Phys. Lett.* **87** 141105
[49] Choquette K D, Lear K L, Schneider R P, Geib K M, Figiel J J and Hull R 1995 Fabrication and performance of selectively oxidized vertical-cavity lasers *IEEE Photo. Technol. Lett.* **7** 1237
[50] Reithmaier J P, Röhner M, Zull H, Schäfer F and Forchel A 1997 Size dependence of confined optical modes in photonic quantum dots *Phys. Rev. Lett.* **78** 378
[51] Bayer M, Gutbrod T, Forchel A, Reithmaier J P, Reinecke T L, Knipp P A, Dremin A A and Kulakovskii V D 1998 Optical modes in photonic molecules *Phys. Rev. Lett.* **81** 2582
[52] Bayer M, Gutbrod T, Forchel A, Reinecke T L, Knipp P A, Werner R and Reithmaier J P 1999 Optical demonstration of a crystal band structure formation *Phys. Rev. Lett.* **83** 5374
[53] Weisbuch C, Nishioka M, Ishikawa A and Arakawa Y 1992 Observation of the coupled exciton-photon mode splitting in a semiconductor quantum microcavity *Phys. Rev. Lett.* **69** 3314
[54] Houdré R, Weisbuch C, Stanley R P, Oesterle U, Pellandini P and Ilegems M 1994 Measurement of cavity-polariton dispersion curve from angle-resolved photoluminescence experiments *Phys. Rev. Lett.* **73** 2043
[55] Ohnesorge B, Bayer M, Forchel A, Reithmaier J P, Gippius N A and Tikhodeev S G 1997 Enhancement of spontaneous emission rates by three-dimensional photon confinement in Bragg microcavities *Phys. Rev.* B **56** R4367
[56] Gutbrod T, Bayer M, Forchel A, Reithmaier J P, Reinecke T L, Rudin S and Knipp P A 1998 Weak and strong coupling of photons and excitons in photonic dots *Phys. Rev.* B **57** 9950–56
[57] Reitzenstein S, Reithmaier J P and Forchel A 2008 Light-matter interaction in single quantum dot – micropillar cavity systems *Semiconductor Quantum Bits* ed O Benson and Henneberger (Singapore: World Scientific)
[58] Reitzenstein S, Hofmann C, Gorbunov A, Strauß M, Kwon S H, Schneider C, Löffler A, Höfling S, Kamp M and Forchel A 2007 $AlAs/GaAs$ micropillar cavities with quality factors exceeding 150 000 *Appl. Phys. Lett.* **90** 251109
[59] Schubert E F 2003 *Light-Emitting Diodes* (Cambridge: Cambridge University Press)
[60] Soltani M, Yegnanarayanan S and Adibi A 2007 Ultra-high Q planar silicon microdisk resonators for chip-scale silicon photonics *Opt. Express* **15** 4695
[61] Gayral B, Gérard J M, Lemaître A, Dupuis C, Manin L and Pelouard J L 1999 High-Q wet-etched GaAs microdisks containing InAs quantum boxes *Appl. Phys. Lett.* **75** 1908
[62] Srinivasan K and Painter O 2007 Mode coupling and cavity-quantum-dot interactions in a fiber-coupled microdisk cavity *Phys. Rev.* A **75** 023814
[63] Rastelli A, Ulhaq A, Kiravittaya S, Wang L, Zrenner A and Schmidt O G 2007 In situ laser microprocessing of single self-assembled quantum dots and optical microcavities *Appl. Phys. Lett.* **90** 073120
[64] Kiravittaya S, Benyoucef M, Zapf-Gottwick R, Rastelli A and Schmidt O G 2006 Ordered GaAs quantum dot arrays on GaAs(001): single photon emission and fine structure splitting *Appl. Phys. Lett.* **89** 233102
[65] Benyoucef M, Kiravittaya S, Mei Y F, Rastelli A and Schmidt O G 2008 Strongly coupled semiconductor microcavities: a route to couple artificial atoms over micrometric distances *Phys. Rev.* B **77** 035108
[66] Astratov V N *et al* 2007 Whispering gallery resonances in semiconductor micropillars *Appl. Phys. Lett.* **91** 071115
[67] Nowicki-Bringuier Y R, Claudon J, Böckler C, Reitzenstein S, Kamp M, Morand A, Forchel A and Gérard J M 2007 High-Q whispering gallery modes in $GaAs/AlAs$ pillar microcavities *Opt. Express* **15** 17291
[68] Sek G, Hofmann C, Reithmaier J P, Löffler A, Reitzenstein S, Kamp M, Keldysh L V, Kulakovskii V D, Reinecke T L and Forchel A 2006 Investigation of strong coupling between single quantum dot excitons and single photons in pillar microcavities *Physica* E **32** 471
[69] Reitzenstein S *et al* 2006 Coherent photonic coupling of semiconductor quantum dots *Opt. Lett.* **31** 1738
Reitzenstein *et al* 2006 Coherent photonic coupling of semiconductor quantum dots *Opt. Lett.* **31** 3507 (erratum)
[70] Press D, Götzinger S, Reitzenstein S, Hofmann C, Löffler A, Kamp M, Forchel A and Yamamoto Y 2007 Photon

antibunching from a single quantum-dot-microcavity system in the strong coupling regime *Phys. Rev. Lett.* **98** 117402

[71] Strauf S *et al* 2006 Frequency control of photonic crystal membrane resonators by monolayer deposition *Appl. Phys. Lett.* **88** 043116

[72] Happ T D, Tartakovskii I I, Kulakovskii V D, Reithmaier J P, Kamp M and Forchel A 2002 Enhanced light emission of $In_xGa_{1-x}As$ quantum dots in a two-dimensional photonic-crystal defect microcavity *Phys. Rev.* B **66** 041303

[73] Strauf S, Stoltz N G, Rakher M T, Coldren L A, Petroff P M and Bouwmeester D 2007 High-frequency single-photon source with polarization control *Nature Photon.* **1** 704

[74] Böckler C *et al* 2008 Electrically driven high-Q quantum dot-micropillar cavities *Appl. Phys. Lett.* **92** 091107

[75] Reitzenstein S, Bazhenov A, Gorbunov A, Hofmann C, Münch S, Löffler A, Kamp M, Reithmaier J P, Kulakovskii V D and Forchel A 2006 Lasing in high-Q quantum-dot micropillar cavities *Appl. Phys. Lett.* **89** 051107

[76] Ulrich S M, Gies C, Ates S, Wiersig J, Reitzenstein S, Hofmann C, Löffler A, Forchel A, Jahnke F and Michler P 2007 Photon statistics of semiconductor microcavity lasers *Phys. Rev. Lett.* **98** 043906